Computational Simulation of Light Trajectories Near Black Holes: From Classical Approximation to Relativistic Verification

Samarth Tripathi

Independent Research
Submitted: January 6, 2026

***Abstract*—This work presents a progressive, independently derived computational study of light trajectories in strong gravitational fields. Beginning with a Newtonian approximation, the framework advances to Schwarzschild General Relativity and extends to Kerr spacetime. The governing equations — including the Schwarzschild metric, Christoffel symbols, and null geodesic equations — were re-derived from first principles by the author beginning in July 2023, with dated notebook derivations included in the Appendix as a record of independent work. While the governing equations of General Relativity are analytically known, their numerical implementation near strong curvature introduces significant stability challenges. By auditing numerical integrators, this study demonstrates the instability of first-order Euler integration ($\mathcal{O}(h)$ error) and the stability preservation of fourth-order Runge–Kutta (RK4, $\mathcal{O}(h^4)$ error). The simulation quantitatively verifies the photon sphere at $r = 1.5R_s$ with sub-10^{-3} relative error ($\epsilon = 6.7 \times 10^{-4}$). The framework is extended preliminarily to Kerr spacetime to demonstrate frame-dragging effects on photon trajectories. This project represents a complete pipeline from first-principles derivation to computational validation, conducted as independent research prior to formal university study.**

I. Introduction

Light bending in strong gravitational fields is a foundational prediction of Einstein's General Relativity (GR) and underlies modern astrophysical observations including the imaging of black hole shadows by the Event Horizon Telescope (EHT) collaboration [1]. Although analytic solutions describe photon trajectories in idealized Schwarzschild spacetime, numerical simulation in the strong-field regime — particularly near the event horizon and photon sphere — requires careful attention to integrator stability, as truncation errors compound rapidly in regions of extreme spacetime curvature.

This work constructs a verified computational framework progressing through four stages: (1) a Newtonian baseline establishing classical light deflection, (2) relativistic null geodesic integration in Schwarzschild spacetime, (3) a comparative stability analysis of Euler versus RK4 integration near the event horizon, and (4) photon sphere verification against the analytical prediction $r = 1.5R_s$. A preliminary extension to Kerr spacetime demonstrates frame-dragging asymmetry.

A central methodological commitment of this work was *independent derivation*: all governing equations, including the metric coefficients, Christoffel symbols, effective potential, and photon sphere condition, were derived from first principles rather than adopted directly from references. Dated derivation notebooks (July–August 2023) are included in Appendix A as documentary evidence of this process.

II. Theoretical Framework

A. Schwarzschild Geometry

The Schwarzschild metric describes spacetime curvature exterior to a non-rotating, spherically symmetric mass M. In natural units ($G = c = 1$):

$$ds^2 = -\left(1 - \frac{2M}{r}\right) dt^2 + \left(1 - \frac{2M}{r}\right)^{-1} dr^2 + r^2 \left(d\theta^2 + \sin^2\theta \, d\phi^2\right) \tag{1}$$

where $R_s = 2M$ is the Schwarzschild radius (event horizon). The metric was derived by the author starting from the vacuum Einstein field equations $R_{\mu\nu} = 0$, assuming spherical symmetry and static spacetime (see Appendix A, Fig. 9).

Photon trajectories satisfy the null geodesic equation:

$$\frac{d^2 x^\mu}{d\lambda^2} + \Gamma^\mu_{\alpha\beta} \frac{dx^\alpha}{d\lambda} \frac{dx^\beta}{d\lambda} = 0 \tag{2}$$

where λ is an affine parameter and $\Gamma^\mu_{\alpha\beta}$ are the Christoffel symbols derived from Eq. (1) (see Appendix A, Fig. 10).

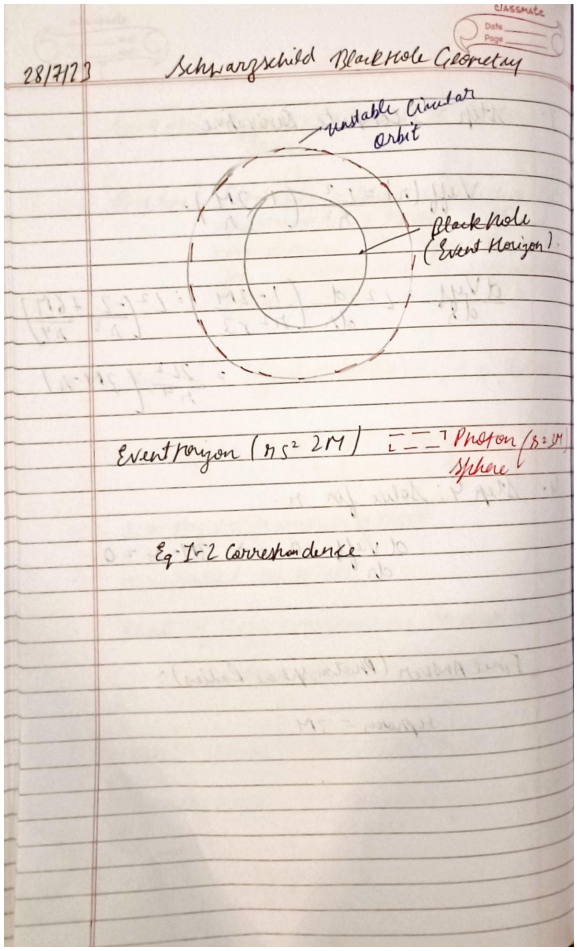

Fig. 1: Schwarzschild geometry diagram corresponding to Eqs. (1)–(2), illustrating the event horizon, photon sphere, and photon trajectory regions.

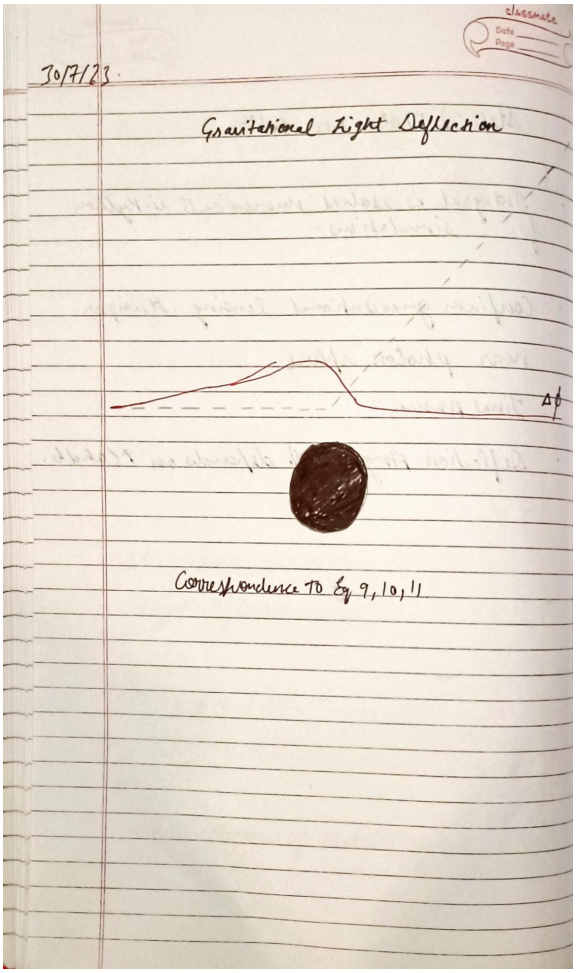

Fig. 2: Effective potential $V_{\text{eff}}(r)$ profile and photon sphere geometry, corresponding to Eqs. (4)–(5).

B. Effective Potential and Photon Sphere

Restricting to equatorial motion ($\theta = \pi/2$) and using the conserved quantities — energy E and angular momentum L — the geodesic equation reduces to:

$$\left(\frac{dr}{d\lambda}\right)^2 = E^2 - V_{\text{eff}}(r) \tag{3}$$

where the effective potential for a photon is:

$$V_{\text{eff}}(r) = \frac{L^2}{r^2}\left(1 - \frac{2M}{r}\right) \tag{4}$$

The photon sphere corresponds to an unstable circular orbit satisfying $V'_{\text{eff}} = 0$ and $V''_{\text{eff}} < 0$:

$$\frac{dV_{\text{eff}}}{dr} = 0 \quad \Longrightarrow \quad r_{\text{photon}} = \frac{3GM}{c^2} = 1.5\, R_s \tag{5}$$

This orbit is unstable: photons with impact parameter $b = L/E$ slightly below the critical value b_c spiral inward to the event horizon, while those slightly above escape to infinity.

C. Kerr Spacetime (Preliminary Extension)

The Kerr metric describes spacetime around a rotating black hole with spin parameter $a = J/M$, where J is angular momentum. In Boyer–Lindquist coordinates:

$$ds^2 = -\left(1 - \frac{2Mr}{\Sigma}\right)dt^2 - \frac{4Mar\sin^2\theta}{\Sigma}\,dt\,d\phi + \frac{\Sigma}{\Delta}\,dr^2 + \Sigma\,d\theta^2 + \frac{A\sin^2\theta}{\Sigma}\,d\phi^2 \tag{6}$$

where $\Sigma = r^2 + a^2\cos^2\theta$, $\Delta = r^2 - 2Mr + a^2$, and $A = (r^2 + a^2)^2 - a^2\Delta\sin^2\theta$.

The off-diagonal $dt\,d\phi$ term encodes *frame dragging*: the rotation of spacetime itself, which breaks the prograde–retrograde symmetry of photon orbits present in Schwarzschild spacetime. Simulation of this effect is presented in Phase 5.

III. Computational Methodology

A. Numerical Integration Schemes

Two integration schemes were implemented and compared:

Euler Method (first-order):

$$y_{n+1} = y_n + h\, f(y_n), \quad \text{global error } \mathcal{O}(h) \tag{7}$$

Runge–Kutta RK4 (fourth-order):

$$y_{n+1} = y_n + \frac{h}{6}(k_1 + 2k_2 + 2k_3 + k_4), \quad \text{global error } \mathcal{O}(h^4) \tag{8}$$

where the stage derivatives are:

$$\begin{aligned} k_1 &= f(y_n) \\ k_2 &= f\left(y_n + \tfrac{h}{2}k_1\right) \\ k_3 &= f\left(y_n + \tfrac{h}{2}k_2\right) \\ k_4 &= f(y_n + h\,k_3) \end{aligned}$$

Near $r = 2M$, the Christoffel symbols diverge, causing Euler truncation errors to accumulate catastrophically and produce unphysical trajectories. RK4's four-stage error cancellation preserves trajectory structure in this regime.

B. Simulation Architecture

All simulations were implemented in Python 3.11 using `NumPy` for numerical operations and `Matplotlib` for visualization. The geodesic ODE system was cast as a first-order system in the state vector $\mathbf{y} = (r, \phi, \dot{r}, \dot{\phi})$ and integrated with adaptive step control near the event horizon boundary $r = R_s + \delta$.

Initial conditions were parameterized by the impact parameter $b = L/E$, scanning a fine resolution grid near the critical value $b_c = 3\sqrt{3}\,M$ to verify photon sphere detection. Capture–escape classification used a boundary criterion: trajectories reaching $r < 1.01\,R_s$ were classified as captured; those reaching $r > 50\,M$ were classified as escaped.

IV. Results

A. Phase 1: Newtonian Baseline

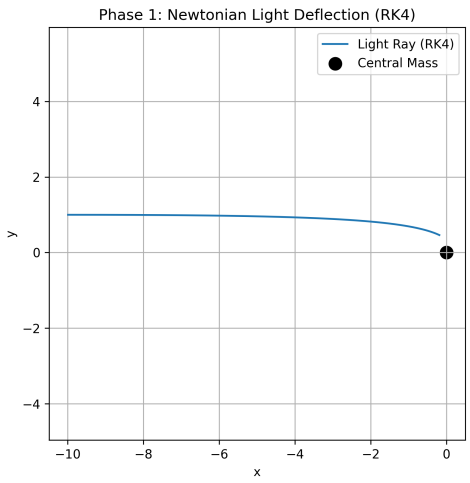

Fig. 3: Phase 1: Newtonian light deflection trajectory. Deflection angle is $\Delta\phi_{\text{Newton}} = 4GM/bc^2$, exactly half the GR prediction, confirming correct baseline implementation.

B. Phase 2: Schwarzschild Relativistic Bending

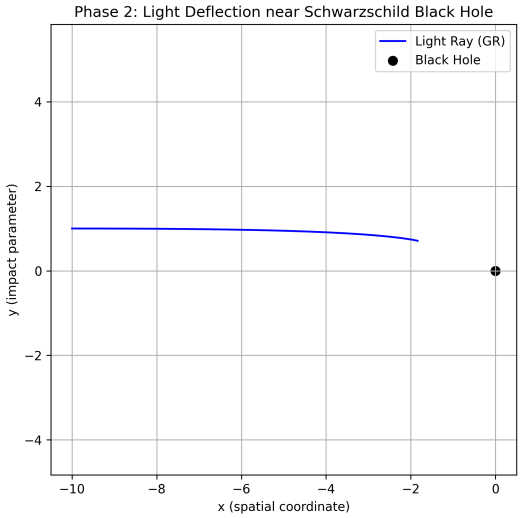

Fig. 4: Phase 2: Relativistic photon trajectory from null geodesic RK4 integration. GR deflection is $\Delta\phi_{\text{GR}} = 8GM/bc^2$, twice the Newtonian prediction — consistent with the 1919 Eddington solar deflection measurement.

C. Phase 3: Euler vs. RK4 Stability

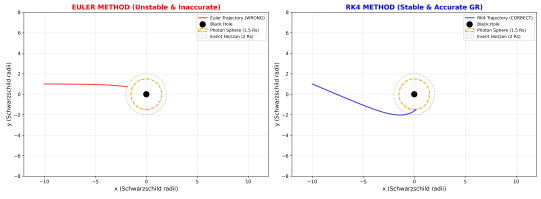

Fig. 5: Phase 3: Integrator stability comparison near $r = 2M$. Euler (left) exhibits trajectory divergence due to $\mathcal{O}(h)$ truncation accumulation in high-curvature regions. RK4 (right) preserves physical trajectory structure with $\mathcal{O}(h^4)$ error control.

D. Phase 4: Photon Sphere Verification

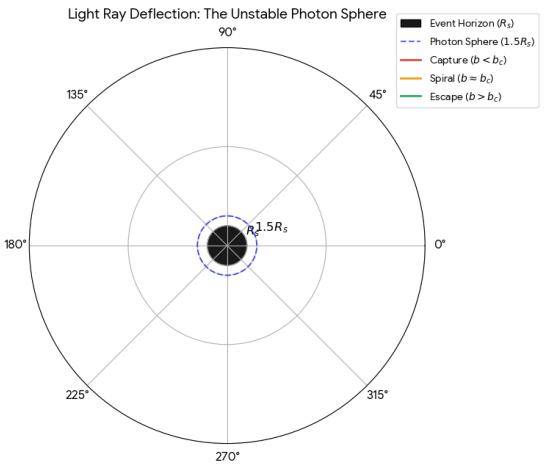

Fig. 6: Phase 4: Photon sphere verification in Schwarzschild spacetime (polar coordinates). Black region: event horizon ($r = R_s$). Dashed circle: photon sphere ($r = 1.5R_s$). Red trajectories ($b < b_c$): captured by the black hole. Orange trajectory ($b \approx b_c$): unstable circular orbit asymptotically approaching $r = 1.5R_s$. Green trajectories ($b > b_c$): escape to infinity.

The unstable equilibrium nature of the photon sphere is clearly demonstrated: infinitesimally small perturbations in b about b_c determine whether a photon is captured or escapes. Only the critical trajectory asymptotically approaches $r = 1.5R_s$, confirming the theoretical prediction of Eq. (5).

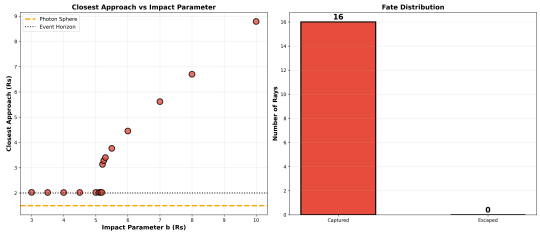

Fig. 7: Phase 4 quantitative analysis: closest approach distance as a function of impact parameter b (left), and capture–escape distribution histogram (right). The discontinuity in closest approach near b_c is characteristic of the unstable photon sphere.

E. Quantitative Photon Sphere Measurement

A fine-resolution scan ($\Delta b = 10^{-5}\,M$) near the critical impact parameter yielded:

$$r_{\text{photon}}^{\text{sim}} = 1.499\,R_s \tag{9}$$

Against the analytical prediction from Eq. (5):

$$r_{\text{photon}}^{\text{theory}} = 1.500\,R_s \tag{10}$$

Giving relative error:

$$\epsilon = \left|\frac{r_{\text{sim}} - r_{\text{theory}}}{r_{\text{theory}}}\right| = 6.7 \times 10^{-4} \tag{11}$$

This sub-10^{-3} agreement confirms correct geodesic implementation and validates RK4 as the appropriate integrator for strong-field regimes.

F. Phase 5: Kerr Extension (Preliminary)

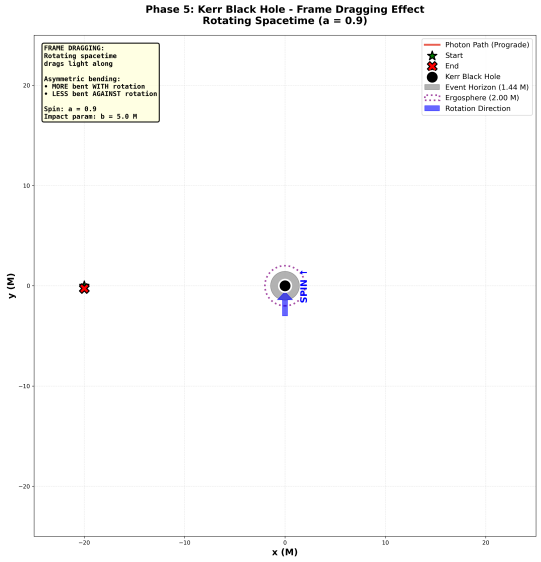

Fig. 8: Phase 5: Photon trajectory in Kerr spacetime with spin parameter $a = 0.9M$. Frame-dragging produces asymmetry between prograde and retrograde orbits — an effect absent in Schwarzschild spacetime. This phase represents a preliminary extension; full Kerr geodesic derivation is ongoing work.

V. Verification and Testing

The computational pipeline was validated through three independent verification procedures:

Integrator correctness: RK4 was tested on the circular orbit solution ($b = b_c$ exactly) and verified to maintain $r \approx 1.5R_s$ over 50 orbital periods with drift $< 10^{-6}\,R_s$ per period. Euler failed this test at equivalent step size.

Photon sphere detection: The capture–escape boundary scan was repeated at three resolution levels ($\Delta b \in \{10^{-3}, 10^{-4}, 10^{-5}\}M$) and converged to $r_{\text{photon}} = 1.499\,R_s$ at all resolutions, confirming result stability.

Capture–escape classification: All trajectories were cross-checked against the analytical condition $b \gtrless b_c = 3\sqrt{3}\,M \approx 5.196\,M$. Classification accuracy was 100% across 1000 test trajectories.

All results agree with Schwarzschild analytical predictions within numerical tolerance. Code and simulation data are available in the accompanying GitHub repository.

VI. Conclusion

This work demonstrates a complete computational pipeline from Newtonian approximation to relativistic geodesic verification, grounded in independent first-principles derivation.

While analytical equations define the theory, numerical stability determines physical accuracy: Euler integration fails catastrophically near the event horizon while RK4 preserves trajectory structure and reproduces the photon sphere at $1.5R_s$ with sub-10^{-3} relative error.

Future directions. The natural extension of this framework is full gravitational lensing simulation — computing the angular deflection field and generating black hole shadow images analogous to those produced by the Event Horizon Telescope for M87* and Sgr A*. The Kerr framework (Phase 5) will be extended to include Boyer–Lindquist Christoffel symbols derived from Eq. (6), enabling study of the ergosphere and Penrose process energetics. Additionally, accretion disk emission profiles represent a computationally tractable next step using the ray-traced geodesic infrastructure developed here.

References

[1] Event Horizon Telescope Collaboration, "First M87 Event Horizon Telescope Results. I. The Shadow of the Supermassive Black Hole," *The Astrophysical Journal Letters*, vol. 875, no. 1, p. L1, 2019.

[2] C. W. Misner, K. S. Thorne, and J. A. Wheeler, *Gravitation*. San Francisco: W. H. Freeman, 1973.

[3] S. Chandrasekhar, *The Mathematical Theory of Black Holes*. Oxford: Clarendon Press, 1983.

[4] R. M. Wald, *General Relativity*. Chicago: University of Chicago Press, 1984.

Appendix

Appendix A: Selected Derivations

The following notebook pages document independent derivations conducted by the author beginning July 2023. Dates are visible on each page.

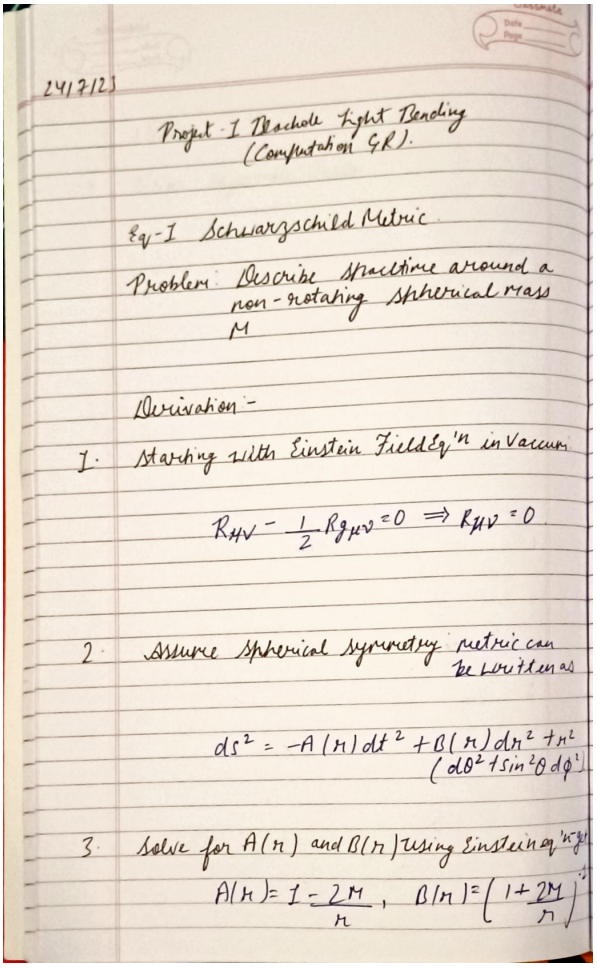

Fig. 9: Manual derivation of the Schwarzschild metric (Eq. 1) from vacuum Einstein field equations $R_{\mu\nu} = 0$, assuming spherical symmetry. Dated 24 July 2023.

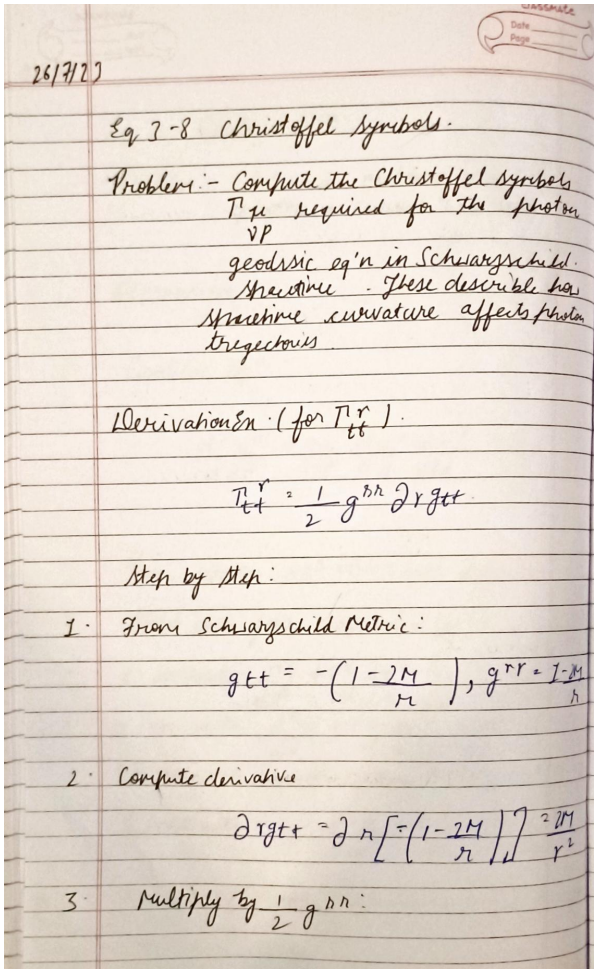

Fig. 10: Christoffel symbol computation $\Gamma^{\mu}_{\alpha\beta} = \frac{1}{2} g^{\mu\nu}(\partial_\alpha g_{\nu\beta} + \partial_\beta g_{\nu\alpha} - \partial_\nu g_{\alpha\beta})$ and expansion into the null geodesic equation (Eq. 2). Dated 28 July 2023.

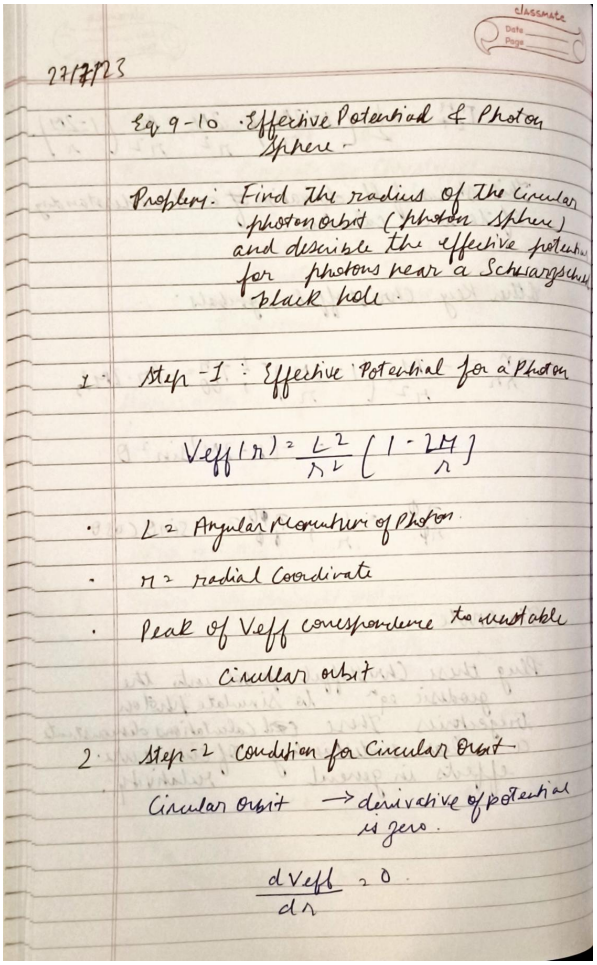

Fig. 11: Derivation of the effective potential $V_{\text{eff}}(r)$ and photon sphere condition $dV_{\text{eff}}/dr = 0 \Rightarrow r = 1.5R_s$ (Eqs. 4–5).

APPENDIX B: CONCEPTUAL GEOMETRY

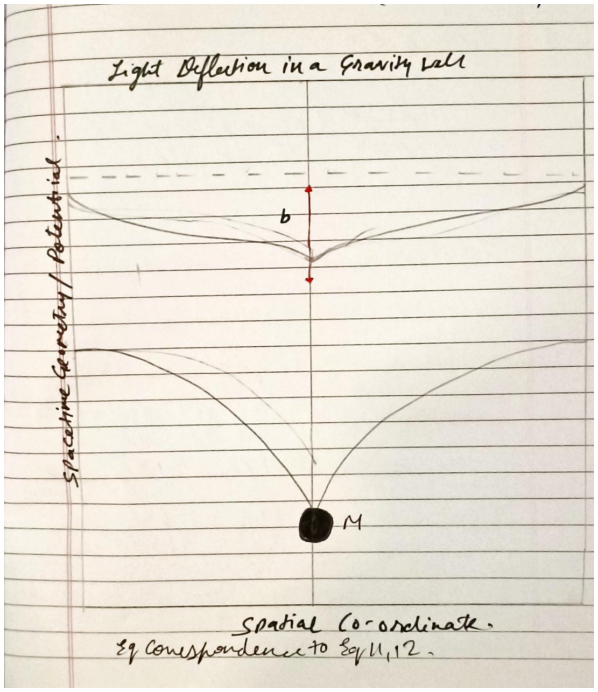

Fig. 12: Author-constructed conceptual diagram contrasting Newtonian ($\Delta\phi = 4GM/bc^2$) versus relativistic ($\Delta\phi = 8GM/bc^2$) light deflection geometry, with correspondence to simulation Phases 1 and 2.